Bulletin of the Seismological Society of America, 91, 3, pp. 520–531, June 2001

Memory-Efficient Simulation of Anelastic Wave Propagation

by Steven M. Day and Christopher R. Bradley

Abstract Realistic anelastic attenuation can be incorporated rigorously into finite difference and other numerical wave propagation methods using internal or memory variables. The main impediment to the realistic treatment of anelastic attenuation in 3D is the very large computational storage requirement imposed by the additional variables. We previously proposed an alternative to the conventional memory-variable formulation, the method of coarse-grain memory variables, and demonstrated its effectiveness in acoustic problems. We generalize this memory-efficient formulation to 3D anelasticity and describe a fourth-order, staggered-grid finite-difference implementation. The anelastic coarse-grain method applied to plane wave propagation successfully simulates frequency-independent Q_p and Q_s. Apparent Q values are constant to within 4% tolerance over approximately two decades in frequency and biased less than 4% from specified target values. This performance is comparable to that achieved previously for acoustic-wave propagation, and accuracy could be further improved by optimizing the memory-variable relaxation times and weights. For a given assignment of relaxation times and weights, the coarse-grain method provides an eight-fold reduction in the storage requirement for memory variables, relative to the conventional approach. The method closely approximates the wavenumber-integration solution for the response of an anelastic half-space to a shallow dislocation source, accurately calculating all phases including the surface-diffracted *SP* phase and the Rayleigh wave. The half-space test demonstrates that the wave field-averaging concept underlying the coarse-grain method is effective near boundaries and in the presence of evanescent waves. We anticipate that this method will also be applicable to unstructured grid methods, such as the finite-element method and the spectral-element method, although additional numerical testing will be required to establish accuracy in the presence of grid irregularity. The method is not effective at wavelengths equal to and shorter than 4 grid cell dimensions, where it produces anomalous scattering effects. This limitation could be significant for very high-order numerical schemes under some circumstances (i.e., whenever wavelengths as short as 4 grids are otherwise within the usable bandwidth of the scheme), but it is of no practical importance in our fourth-order finite-difference implementation.

Introduction

Finite-difference (FD), finite-element, spectral-element, and pseudospectral methods are currently able to solve transient three-dimensional seismic-wave propagation problems over domains sufficiently large that anelastic attenuation should be included. Realistic treatment of anelastic losses is especially important for simulating the earthquake-induced response of complex geologic structures such as sedimentary basins (e.g., Frankel and Vidale, 1992; Yomogida and Etgen, 1993; Olsen and Archuleta, 1996; Wald and Graves, 1998; Pitarka *et al.,* 1998; Sato *et al.,* 1999; Olsen *et al.,* 2000). An important component of the ground motion in basins is the trapping of incident waves at the basin edges, resulting in the excitation of surface waves in the basin sediments (e.g., Field, 1996; Boore, 1999). These basin-edge-induced waves in turn may reverberate within the basin. Numerical simulations that neglect anelastic losses in the sediments may seriously overpredict the amplitude and duration of the ground motion, even if the seismic velocity structure and source are well modeled. Realistic formulation of anelastic losses is also important in other applications of 3D numerical simulations. These include studies directed at seismic verification of the comprehensive test ban treaty. The latter studies have employed full waveform simulations over regional crustal paths, and these simulations are strongly affected by

both intrinsic and scattering attenuation (Al-Kahtib and Mitchell, 1991; Jones *et al.,* 1998; Mitchell, *et al.,* 1997). Additionally, 3D modeling of seismic reflection profiles (e.g., Carcione *et al.,* 1992), and global-scale seismic waveform modeling (e.g., Igel and Weber, 1995; Yoon and McMechan, 1995; Chaljub and Vilotte, 1998; Komatitsch and Tromp, 2000) require realistic and computationally tractable treatment of attenuation.

A fully general formulation of anelasticity represents stress at ($\mathbf{x}$, t) as a convolution of the time history of strain at $\mathbf{x}$ with a relaxation function, which can be specified in terms of the corresponding relaxation spectrum (e.g., Nowick and Berry, 1972). This convolutional form of the stress-strain operator is not useful for time-domain numerical simulations, however, because it would require enormous storage for the strain histories and an impossibly large computational load to execute the convolutions. Anelastic losses can be incorporated into time-stepped numerical methods (such as the FD method) practically, yet rigorously, by introducing a set of internal or memory variables at each stress node point (Day and Minster, 1984). The evolution of each memory variable is governed by a linear, constant-coefficient, first-order differential equation analogous to that governing the standard linear solid (e.g., Day and Minster, 1984; Emmerich and Korn, 1987; Carcione *et al.,* 1988; Witte and Richards, 1990; Krebs and Quiroga-Goode, 1994; Blanch *et al.,* 1995; Xu and McMechan, 1995). Each memory variable represents a distinct relaxation process and is associated with a distinct relaxation time, and the superposition of several memory variables can be used to approximate the relaxation function appropriate to the material being modeled. Day and Minster (1984) prove that, for any continuous relaxation spectrum, the corresponding linear operator that maps strain history into stress can be uniformly approximated using a set of discrete relaxation times (and therefore a discrete set of memory variables).

The benefit of the memory variable formulation is that only the current value of each of the N memory variables need be stored (along with the other field variables, typically the stress and velocity components), because the current value is sufficient to permit its first-order ordinary differential equation (ODE) to be stepped forward in time. If N is small, the added memory requirement (relative to lossless elasticity) and computational load may not be prohibitive.

The challenge in implementing the memory variables approach is that seismological and laboratory observations usually imply an anelastic quality factor (Q) for rock that is at most weakly dependent on frequency and often well approximated by a constant. This in turn implies a relaxation function with a broad spectrum of relaxation times (e.g., Lomnitz, 1957). Each memory variable contributes only a single relaxation time to the relaxation function. In order to approximate a constant Q over a given frequency band, it has been found in practice that two to three memory variables are required per decade of bandwidth. This requirement applies to each stress component and to each computational unit cell. In three-dimensional anelasticity, for example, where there are six independent stress components, roughly two to three dozen additional stored variables per unit cell would be required to achieve two decades of nearly constant Q.

Day (1998) (hereafter D98) proposed an alternative formulation he referred to as coarse-grain memory variables. In this formulation, there is only a single memory variable per stress component per unit cell, but a fast spatial scale is introduced over which the relaxation time varies. The wave field spatially averages the relaxation processes over the fast scale, resulting in a good approximation to frequency-independent Q. It was shown in D98 that this method performs well in FD solutions of the scalar-wave equation, achieving constant Q within a 3% tolerance over two decades in frequency. If a precise representation of Q is only required over a narrower bandwidth, the number of memory variables can be reduce to even fewer than one per unit cell (per stress component), potentially reducing memory usage to only fractionally more than that of purely elastic calculations.

In this article, we extend the coarse-grain memory variable approach to anelastic wave propagation in three dimensions. The method is implemented in a fourth-order, staggered-grid FD program, and we verify its accuracy for plane P and S waves. We then show, by comparison with a wavenumber-integration solution, that the method also gives accurate solutions for the response of an anelastic half-space to a shallow dislocation source. The half-space response includes strongly excited surface-diffracted *SP* and Rayleigh-wave phases, each of which is reproduced with accuracy comparable to that achieved in the elastodynamic (infinite Q) case. This result demonstrates that the averaging concept underlying the method is still effective near boundaries and in the presence of evanescent waves.

Background

This section first reviews the conventional memory variable formulation and its relationship to the relaxation spectrum and to the frequency dependence of Q. Then we review the coarse-grain alternative of D98. Finally, we review the performance and limitations of the coarse-grain approach noted by D98 for the acoustic case. We adhere to the notation of D98, using M to denote the time-dependent modulus, that is, the step response of the stress-strain relationship, namely

$$\sigma(t) = \int_0^t M(t - t')d\varepsilon(t'), \tag{1}$$

where σ is the stress and ε is the strain. The unrelaxed modulus M_u, the relaxed modulus M_R, the relaxation of the modulus, δM and the normalized relaxation function ϕ, are given by

$$M_u = M(0), \tag{2}$$

$$M_R = M(\infty), \tag{3}$$

$$\delta M = M_u - M_R, \tag{4}$$

and

$$M(t) = M_R + \delta M \phi(t). \tag{5}$$

The relaxation function can be written in terms of a relaxation spectrum Φ:

$$\phi(t) = \int_{-\infty}^{\infty} e^{-t/\tau} \Phi(\ln \tau) d(\ln \tau) \tag{6}$$

(Nowick and Berry, 1972).

Conventional Memory Variable Method

We approximate the continuous relaxation spectrum with a discrete spectrum:

$$\Phi(\ln \tau) \approx \sum_{i=1}^{N} \lambda_i \delta(\ln \tau - \ln \tau_i), \tag{7}$$

where τ_i is a relaxation time, λ_i is the relative strength of the corresponding relaxation, and N is the number of relaxation terms in the approximation. As noted by Day and Minster (1984), the τ_i and λ_i can also be interpreted as the poles and residues, respectively, of the operational modulus, namely, the Laplace transform of $M(t)$, after the approximation implied by equation (7) has been introduced. As shown by Day and Minster (1984), and in the current notation in D98, equations (1) through (7) are equivalent to the stress-strain relationship

$$\sigma(t) = M_u \left[\varepsilon(t) - \sum_{i=1}^{N} \zeta_i(t) \right], \tag{8}$$

in which the ζ_i, $i = 1 \ldots, N$ are internal, or memory, variables that evolve, respectively, according to the N first-order differential equations

$$\tau_i \frac{d\zeta_i(t)}{dt} + \zeta_i(t) = \lambda_i \frac{\delta M}{M_u} \varepsilon(t), \tag{9}$$

which are specified by the $2N$ values of τ_i and λ_i, $i = 1, \ldots, N$. The corresponding approximation to $Q^{-1}(\omega)$ is (in the low-loss approximation)

$$Q^{-1}(\omega) \approx \frac{\delta M}{M_u} \sum_{i=1}^{N} \frac{\lambda_i \omega \tau_i}{\omega^2 \tau_i^2 + 1}. \tag{10}$$

In the conventional memory variables approach, $2N$ values of τ_i and λ_i are chosen in such a way that equation (10) is a good approximation to some target $Q^{-1}(\omega)$. Typically, the target is a constant Q over a specified bandwidth, although the power laws $Q = Q_0 \omega^{\nu}$ are sometimes of interest. Various schemes have been developed to optimize the approximation of constant Q (e.g., Emmerich and Korn, 1987; Carcione *et al.,* 1988; Witte and Richards, 1990; Krebs and Quiroga-Goode, 1994; Blanch *et al.,* 1995; Xu and McMechan, 1995). An approximation to frequency-independent Q that is adequate for most applications can be obtained with roughly one memory variable per octave (Robertsson *et al.,* 1994; Blanch *et al.,* 1995).

The additional storage required for the memory variables can easily become the dominant factor limiting problem size, particularly in 3D where there are six stress components (and therefore $6N$ memory variables per unit cell). For example, achieving nearly constant Q over two decades in frequency in a 3D FD wave propagation calculation roughly quadruples the storage for anelastic simulations, compared with perfectly elastic simulations (D98). The composite memory variables approach of Xu and McMechan (1995) can reduce the memory variable storage by a factor of 2 by storing only those linear combinations of the conventional memory variables that appear in the equations of motion. However, for the preceding example, which is representative of the kind of anelastic simulation that is of interest in seismological applications, memory variables will still dominate the storage requirements.

Coarse-Grain Memory Variables

D98 proposed an alternative to using N relaxation times τ_i and strengths λ_i (and therefore N corresponding memory variables) at each point to approximate the relaxation spectrum on a pointwise basis. The D98 alternative is to use only a single relaxation (and memory variable) at each point, but permit that relaxation time, together with a weighting function, to vary spatially over a fast spatial scale. By fast scale we mean that the scale length of the variations is shorter than the minimum wavelength of the wave field (but larger than the computational unit cell size of the spatial discretization). When we introduce this weighted spatial dependence into the relaxation equation (9), it becomes

$$\tau(\mathbf{x}) \frac{d\zeta(\mathbf{x}, t)}{dt} + \zeta(\mathbf{x}, t) = w(\mathbf{x}) \frac{\delta M}{M_u} \varepsilon(\mathbf{x}, t) \tag{11}$$

where w is the weighting function. The stress is then the sum of the instantaneous elastic response plus a single memory term ζ:

$$\sigma(x, t) = M_u[\varepsilon(x, t) - \zeta(x, t)]. \tag{12}$$

The fast or subwavelength scale spatial dependence, shown explicitly in equation (11), is used to simulate the target

relaxation spectrum and not to model real spatial variations in material properties. There is also implicit in equation (11) a slow scale, over which $\delta M/M_u$ may vary if we wish to model real spatial variations in Q. We suppress this slow scale in the notation because our focus is on the use of the fast scale to simulate the relaxation spectrum [and thereby $Q(\omega)$].

D98 gave a prescription (equations 18–21 of D98) for the construction of $\tau(\mathbf{x})$ and $w(\mathbf{x})$ in terms of the target relaxation spectrum. In that article, it was argued, from perturbation theory, that a model equation (11) following this prescription should reproduce the target $Q(\omega)$ if $\tau(\mathbf{x})$ and $w(\mathbf{x})$ are periodic in space with a spatial period shorter than 1/2 the minimum wavelength of interest. The D98 method thus mimics the actual physical origin of the relaxation spectra of earth materials (i.e., heterogeneity at the microscopic level) but on a coarser, though still subwavelength scale.

Implementation for Acoustic Case

D98 also gave a practical coarse-grain implementation for the acoustic wave equation, discretized on a 3D lattice. In that implementation, the relaxation spectrum is first approximated in the form (7), with N equal to 8. Then $\tau(\mathbf{x})$ takes the eight different discrete values τ_k, $k = 1, \ldots, 8$, and these are assigned to the stress node points in a periodic array, with the period in each lattice direction equal to twice the corresponding principal lattice period. The eight values of $w(\mathbf{x})$, w_k, are given by the eight relaxation strengths λ_k in equation (7) but normalized to have unit volumetric mean. The normalization of the relaxation function implied by equation (5) then requires $w_k = 8\ \lambda_k$. The w_k values are assigned in the same 3D periodic array as the τ_k values.

To approximate the special case of frequency-independent Q, D98 used values of τ_k equally spaced on a logarithmic scale between lower and upper absorption-band cutoffs τ_m and τ_M, respectively. All weights w_k were set to 1. In the acoustic case, the appropriate modulus in equation (9) is the bulk modulus κ, and the bulk modulus relaxation $\delta\kappa/\kappa_u$ was set such that the specified constant Q value, Q_0, is realized at some prescribed reference frequency ω_0 (near the center of the absorption band). The appropriate $\delta\kappa/\kappa_u$ then satisfies

$$Q_0^{-1} \approx \frac{\pi\delta\kappa}{2\kappa_u}\left[\ln\left(\frac{\tau_M}{\tau_m}\right) + \frac{\delta\kappa}{\kappa_u}\ln\left(\omega_0\tau_m\right)\right]^{-1}. \quad (13)$$

This procedure successfully simulates frequency-independent Q, to within 3% tolerance, over 2 orders of magnitude in frequency, yet requires only one memory variable per stress node. A limitation of the method is that it produces strong scattering at wavelengths shorter than 4 grid cells (as predicted by the perturbation analysis and confirmed by numerical experiments in D98). As a result, the method is probably most appropriate for use with relatively low-order FD and finite-element methods, for which wavelengths shorter than 4 grid cells are already subject to large errors due to numerical dispersion. On the basis of acoustic wave tests in D98, the method appears to be well suited to the fourth-order staggered-grid FD method that is now widely used in seismological applications.

Anelastic Formulation

The coarse representation of the relaxation spectrum is easily generalized from the acoustic to the anelastic case, and the generalization is particularly simple for isotropic anelasticity, to which we limit ourselves in this article. In the isotropic case, the stress-strain relationship can be partitioned into separate relationships of the form of equation (12) for the mean stress $\sigma_{kk}/3$ (in terms of the volumetric strain ε_{kk}, a volumetric memory variable, and bulk modulus, κ), and the deviatoric stresses σ'_{ij} (in terms of the deviatoric strains ε'_{ij}, corresponding memory variables, and shear modulus μ), respectively. Considering that only five of the six deviatoric stress (and strain) components are independent, this formulation leads to one equation of the form of equation (11) for each of six memory variables. For example, adding attenuation to a 3D staggered-grid FD method (assuming a conventional velocity-stress formulation, e.g., Graves [1996]) requires adding six memory variables to each unit cell of the grid.

In the aforementioned formulation, one could assign different frequency dependencies to the compressional and shear Q values, $Q_\kappa(\omega)$ and $Q_\mu(\omega)$, respectively. This assignment would be accomplished by using one set of τ_k and w_k in the equation controlling the memory variable for mean stress, and a different set in the five equations controlling the memory variables associated with the deviatoric stresses. The development is less cumbersome, however, if we make the additional assumption that $Q_\kappa(\omega)$ and $Q_\mu(\omega)$ share a common frequency dependence. That is, we assume that their ratio is a frequency-independent constant, $Q_{\kappa 0}/Q_{\mu 0}$ (that may vary spatially, however). In that case, there is one common set of relaxation times and weights (but, in general, different modulus relaxations, $\delta\kappa/\kappa_u$ and $\delta\mu/\mu_u$, respectively) for the mean stress and deviatoric stress versions of equation (11). One advantage of this simplification is that we can avoid partitioning the stress tensor into mean stress and deviatoric stress parts. Instead, we form linear combinations of the mean stress and deviatoric stress memory variables, choosing combinations that correspond to the usual physical components of the total stress tensor. A second advantage is that we can then write the memory variable evolution equation (11) in terms of the modulus relaxations $A_p \equiv \delta(\kappa + 4\mu/3)/(\kappa + 4\mu/3)_u$ and $A_s \equiv \delta\mu/\mu_u$, which can be related to the Q values for P and S waves, Q_p and Q_s, respectively.

The above procedure is detailed in the Appendix and leads to the following set of equations:

$$\sigma_{ij} = 2\mu_u\varepsilon_{ij} + \left(\kappa_u - \tfrac{2}{3}\mu_u\right)\varepsilon_{kk}\delta_{ij} - \xi_{ij}, \quad (14)$$

and

$$\tau \frac{d\xi_{ij}}{dt} + \xi_{ij} = w\Big[2\mu_u A_s \varepsilon_{ij} + \Big[\Big(\kappa_u + \tfrac{4}{3}\mu_u\Big)A_p - 2\mu_u A_s\Big]\varepsilon_{kk}\delta_{ij}\Big], \quad (15)$$

where A_p and A_s are constants that scale with Q_p^{-1} and Q_s^{-1}, respectively. For the special case of nearly frequency-independent Q, these constants are

$$A_p = \frac{2}{\pi} Q_{p0}^{-1} \left(\ln \frac{\tau_M}{\tau_m}\right) \left[1 - \frac{2}{\pi} Q_{p0}^{-1} (\ln \omega_0 \tau_m)\right]^{-1}, \quad (16)$$

and

$$A_s = \frac{2}{\pi} Q_{s0}^{-1} \left(\ln \frac{\tau_M}{\tau_m}\right) \left[1 - \frac{2}{\pi} Q_{s0}^{-1} (\ln \omega_0 \tau_m)\right]^{-1}, \quad (17)$$

where Q_{p0} and Q_{s0} are the Q values at reference frequency ω_0. In equations (15) to (17), τ_M, τ_m, and ω_0 are time-independent constants. The variables Q_p, Q_s, μ_u, and κ_u are time independent but vary on the slow spatial scale, namely, the scale representing actual physical variations of the model. The variables τ and w are time independent but vary on the fast scale, namely, the scale representing the coarse graining to simulate the relaxation spectrum (and do not vary on the slow spatial scale). The six anelastic memory variables ξ_{ij} are time dependent and vary on both spatial scales.

Staggered-Grid Finite-Difference Implementation

We incorporate coarse-grain anelasticity into a 3D staggered-grid FD method. The implementation is analogous to that used in D98 for the acoustic case. The underlying elastodynamic code, that of Olsen (1994), uses the velocity-stress formulation in which the three velocity components and six stress components are the dependent variables. This method approximates spatial derivatives with fourth-order accuracy and time derivatives with second-order accuracy. Graves (1996) gives a detailed description of the difference equations, and our formulation differs from that formulation only in the location of the free surface within the unit cell. We use the free-surface formulation that Graves calls the "zero-stress" formulation but with the roles of shear and normal stress interchanged relative to Graves (1996, equation [15]).

Figure 1 summarizes the geometrical structure of the anelastic program. At each time step, the program uses the nodal velocities to approximate the strain rate $\dot{\varepsilon}_{ij}$. The time-differentiated form of equation (15) provides a first-order ODE to be solved for the (time-differentiated) memory variable $\dot{\xi}_{ij}$, given the $\dot{\varepsilon}_{ij}$ values. Then, the time-differentiated form of equation (14) gives an expression for the stress rate $\dot{\sigma}_{ij}$ in terms of the $\dot{\varepsilon}_{ij}$ values and $\dot{\xi}_{ij}$ values. The only changes from the perfectly elastic program are the following: (1) six new variables (the memory variables $\dot{\xi}_{ij}$) are assigned to each unit cell; (2) each unit cell is assigned one of eight relaxation times τ_k and one of the eight associated weights w_k in an arrangement described later; (3) the elastic stress-strain relation is augmented by the term $-\dot{\xi}_{ij}$, giving equation (14) (in time-differentiated form); and (4) memory variable $\dot{\xi}_{ij}$ is updated at each time step by solving a difference approximation to equation (15) (in time-differentiated form).

The values of τ_k and w_k depend upon the attenuation model, and we give specifics for the special case of frequency-independent Q later. Once these values have been specified, they are distributed in the grid according to the following scheme. Grid unit cells are indexed by the three integers p, q, r, such that a reference point in each cell center is located at vector position $\mathbf{x}_{pqr} = p\mathbf{a}_1 + q\mathbf{a}_2 + r\mathbf{a}_3$, where $\mathbf{a}_j$ ($j = 1, 2, 3$) are the lattice vectors of the grid. Then the cell at $\mathbf{x}_{pqr}$ is assigned τ_k, where $k = 1 + p \bmod 2 + 2(q \bmod 2) + 4(r \bmod 2)$, namely,

$$\tau(\mathbf{x}_{pqr}) = \tau_{1+p \bmod 2+2(q \bmod 2)+4(r \bmod 2)}, \quad (18)$$

and similarly for w,

$$w(\mathbf{x}_{pqr}) = w_{1+p \bmod 2+2(q \bmod 2)+4(r \bmod 2)}. \quad (19)$$

The p, q, and r can be permuted arbitrary in equations (18) to (19) without making any essential difference to the method. The arrangement (18) is sketched in Figure 1.

Equation (15) is solved using a simplification of the difference equation approximation given in D98 (see equation [14] in D98). The simplification is the same one used by Day and Minster (1984), and consists of approximating the exponential by its first diagonal Padé approximant, namely, $e^{-x} \approx (1 - \frac{x}{2})/(1 + \frac{x}{2})$. The result is

$$\dot{\xi}_{ij}(t + \delta t) = \frac{\left(\tau_k/\delta t - \frac{1}{2}\right)\dot{\xi}_{ij}(t) + \frac{1}{2}[f(t) + f(t + \delta t)]}{\left(\tau_k/\delta t + \frac{1}{2}\right)} \quad (20)$$

where

$$f(t) = w_k \Big\{2\mu_u A_s \dot{\varepsilon}_{ij}(t) + \Big[\Big(\kappa_u + \tfrac{4}{3}\mu_u\Big)A_p - 2\mu_u A_s\Big]\dot{\varepsilon}_{ll}(t)\delta_{ij}\Big\} \quad (21)$$

We have not written out the spatial dependence in equations (20) to (21), since all quantities are evaluated at the same

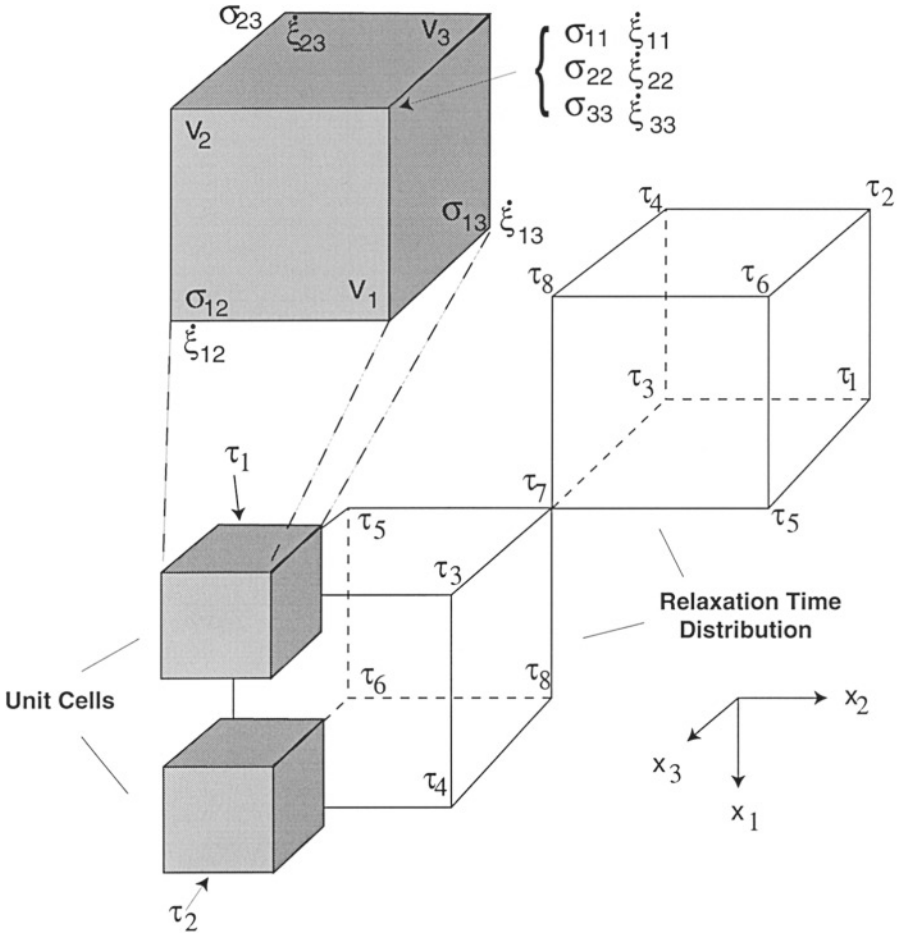

Figure 1. Geometry of the finite-difference grid and the unit cell. Memory variables ξ_{ij} are colocated with the corresponding stresses σ_{ij}. The relaxation times τ_k repeat with spatial period equal to twice the unit cell dimension.

location $\mathbf{x}_{pqr}$. As before, k is the coarse relaxation index $1 + p\text{mod}2 + 2(q\text{mod}2) + 4(r\text{mod}2)$.

The relaxation times and weights depend upon the $Q(\omega)$ model. We present numerical examples for the case of nearly frequency-independent Q, as represented by a relaxation spectrum constant on support interval $(\ln \tau_m, \ln \tau_M)$. D98 showed that the set of relaxation times

$$\ln \tau_k = \ln \tau_m + \frac{2k - 1}{16} (\ln \tau_M - \ln \tau_m) \quad (22)$$

(uniformly distributed over the support interval), with all weights equal to 1, provides a simple, though certainly not optimal, approximation, and we adopt that approximation in this article. In this case of nearly constant Q, A_p and A_s are given by equations (16) and (17), respectively.

A convenient way to specify the bounds of the absorption band, τ_m and τ_M, is in terms of the Nyquist frequency ω_n associated with the computational time step. We adopt the bounds $\tau_m = \omega_n^{-1}$ and $\tau_M = 5N_t\omega_n^{-1}$, where N_t is the total number of time steps in the computation and find that this choice ensures a nearly constant Q throughout the full usable bandwidth of the FD computations.

The above implementation does not depend in any essential way on the particular spatial differencing scheme employed. In Figure 1, we have illustrated the staggered velocity-stress formulation, and it is for this scheme (with fourth-order accurate difference operators) that we compute the numerical examples in the next section. However, the only essential geometrical elements of our implementation are the logically rectangular grid structure, the association of the τ values (and w values) with alternating unit cells (via equations (18) to (19)), and the positioning of each memory variable in coincidence with the corresponding stress component. The formulation therefore generalizes immediately to any logically rectangular structured grid scheme.

Numerical Examples

D98 performed a perturbation analysis that suggests that the coarse-grain method should be accurate for wavelengths exceeding four times the unit cell dimension. Numerical tests

in that article bore out this expectation for the acoustic-wave equation with frequency-independent Q. Numerically simulated plane-wave pulses matched their analytical counterparts to high accuracy, and all numerical artifacts were strictly confined to the frequency band corresponding to wavelengths shorter than four grid cells. The apparent Q in those tests, as a function of frequency, was denoted by $\hat{Q}(\omega)$. It was estimated from the ratio of the pulse spectra at successive locations, by

$$\hat{Q}^{-1}(\omega) = \frac{-2c \ln|u(x + L, \omega)/u(x, \omega)|}{\omega L} \qquad (23)$$

(which corrects a typographical error in equation (48) of D98), where u is the Fourier transformed displacement, c is the wavespeed, and L is the propagation distance. The apparent Q in the acoustic plane-wave tests matched the target Q to within a few percent over more than two decades of frequency.

In this article we perform similar plane-wave numerical tests for the anelastic case. The plane-wave tests will verify that the anelastic algorithm is correctly programmed, of course. However, the plane-wave tests serve a further purpose. The fast-scale variations of $\tau(\mathbf{x})$, which produce short-wavelength artifacts in the acoustic case, will in the anelastic case also produce some coupling among the *P*, *SV*, and *SH* components of plane-wave displacement. It is necessary to verify that any artifacts resulting from the cross-coupling are negligible within the usable bandwidth of the FD method (which we take to be wavelengths exceeding five unit cell dimensions). The plane-wave tests also serve to demonstrate that the cross-coupling does not lead to any numerical instability that might not have been present in the acoustic case.

We then further test the anelastic method by applying it to a shallow point dislocation source in a uniform half-space. This 3D numerical test has the important attribute that the source excites free-surface interface waves of several types, including a Rayleigh wave. Boundary condition implementation often controls overall accuracy for the FD method, and simulation of the uniform half-space Rayleigh wave has frequently proven to be a decisive test of elastodynamic FD techniques.

Plane-Wave Test

We generate plane *P* and *S* waves by imposing a minimum-phase velocity pulse everywhere on one lattice plane of the grid, with motion either normal (*P* wave) or parallel (*S* wave) to the plane. Estimates of the apparent Q values are obtained from spectral ratios of the velocity at successive distances from the source plane, using equation (23), and setting c to the appropriate wavespeed, α (*P*-wave case) or β (*S*-wave case). Results are shown in Figure 2 for the case $Q_{s0} = 50$, $Q_{p0} = 50$, $\alpha/\beta = 3^{1/2}$. The inset shows the successive velocity pulses at distances of 10, 110, and 210 times the grid-cell size δx, for source velocity pulse shape $te^{-t/2\pi T}$. The time unit in the figure is the *S*-wave propagation time across δx; in this unit the characteristic source duration (the inverse corner frequency) T is 22. Velocity is normalized to give unit peak velocity at the source plane. The apparent Q values, $\hat{Q}_p(\omega)$ and $\hat{Q}_s(\omega)$, shown in Figure 2 were obtained from velocities at the first pair of sites, but the results are virtually unchanged if the second pair are used instead.

The apparent Q values are frequency independent to within about 4% over the two decades shown in Figure 2, which covers periods ranging from the full duration of the computation down to the period corresponding to a five-grid *S* wavelength. The nearly constant Q values are biased downward from the target value by a small amount, less than 4%. This is close to the accuracy achieved in the acoustic case (D98), and if higher accuracy is required it should be easy to achieve by optimizing the choice of the weights w_i and relaxation times τ_i, which we have made no attempt to do.

The weak heterogeneity caused by the coarsely represented relaxations produces a small amount of cross talk among components, typically around 2 orders of magnitude smaller in maximum amplitude than the main pulse. This effect does not impair the stability of the computations nor does it seem to have any significant practical consequences, as is further verified in the half-space point source test in the next section. We have done plane-wave tests for Q values ranging from 20 to 300, and ratios Q_{p0}/Q_{s0} ranging from 1 to 2, and the calculations are stable and accurate in all cases.

Half-space Point Source Test

Figure 3 shows the problem geometry for the uniform half-space example. The source is a buried double couple, equivalent to a point shear dislocation with left-lateral slip in the x_1 direction on a vertical plane normal to x_2 axis (with x_3 positive down). The source is at (0 km, 0 km, 2 km). The grid-cell spacing is 100 m, and the time step is 0.008 sec. Grid boundaries (other than the free surface of the half space) are at sufficient distance that they do not influence the first 4 sec of the solution at distances within 10 km of the source. This arrangement was chosen so that we can assess the attenuation methodology without having to account for any added artifacts due to imperfection in the absorbing boundaries at the sides and bottom of the grid. The *P*- and *S*-wavespeeds and density are 6 km/sec, 3.46 km/sec, and 2700 kg/m^3, respectively, and Q_{p0} and Q_{s0} are both 50. The moment rate function $\dot{m}$ of the dislocation source is a Gaussian with spread S:

$$\dot{m}(t) = \frac{M_0 H(t)}{\sqrt{2\pi} S} e^{-0.5(t-4S)^2/S^2}, \qquad (24)$$

(H is the Heaviside step function, and the offset $4S$ is present in the Gaussian argument in order to make the discontinuity at time $t = 0$ negligibly small). For the examples shown below, the source moment M_0 has been scaled to 10^{18} N m.

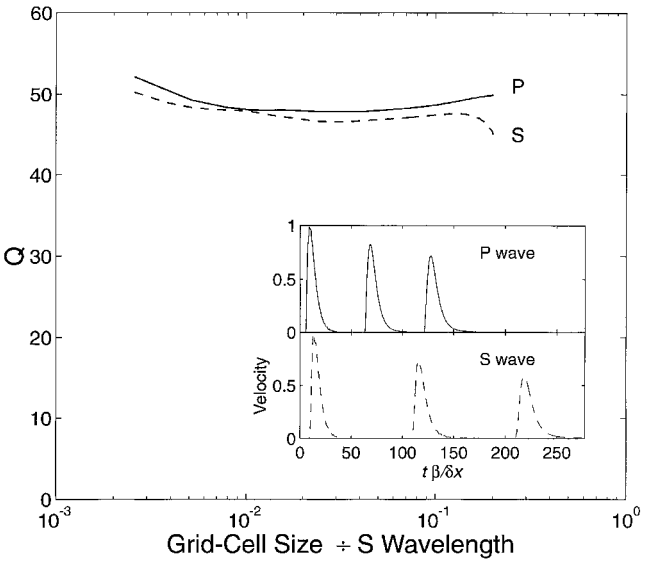

Figure 2. Plane wave test results for Q_p and Q_s of 50. Estimates of Q were obtained from spectral ratios of the velocity waveforms shown in the inset. Timescale is normalized to the *S*-wave travel time across one grid cell ($\beta/\delta x$ is the ratio of *S*-wave speed to cell dimension). Velocity is normalized to have a unit maximum amplitude at the source location.

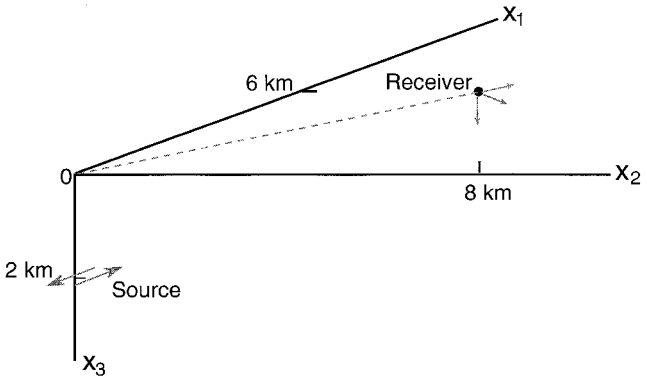

Figure 3. Problem geometry for the uniform half-space numerical example. The source is a point shear dislocation at a 2-km depth, with seismic moment of 10^{18} N m and the moment rate function given by equation (24). Velocity is computed at the free-surface point (6 km, 8 km, 0 km), which is at an epicentral distance of 10 km.

We examine the computed velocity waveforms, at location (6 km, 8 km, 0 km), for the Gaussian spread $S = 0.045$. This value of S is chosen because it is right at the threshold at which the numerical solution in the perfectly elastic case ($Q = \infty$) begins to show visible artifacts due to numerical dispersion. This behavior of the infinite Q case is shown in Figure 4, where the FD solution is compared with a solution obtained by wavenumber integration (Apsel and Luco, 1983). The point of Figure 4 is to verify that, in the lossless case, this source function is sufficiently broadband to exhibit the entire effective (i.e., artifact free) bandwidth of the FD solution on this grid.

To assess the finite Q simulations, a reference solution was again obtained using the wavenumber-integration method of Apsel and Luco (1983). We modified the Apsel and Luco method to include a causal attenuation with a constant relaxation spectrum on ($\ln \tau_m$, $\ln \tau_M$). The modification required replacing the shear modulus in their method with the complex, frequency-dependent modulus $\mu(\omega)$,

$$\mu(\omega) = \mu_u \left(1 - \frac{1}{\pi Q_{s0}} \ln \frac{\tau_M^2 + \omega^2\tau_m^2\tau_M^2}{\tau_m^2 + \omega^2\tau_m^2\tau_M^2} + \frac{2i}{\pi Q_{s0}} \tan^{-1} \frac{\omega(\tau_M - \tau_m)}{1 + \omega^2\tau_m\tau_M}\right), \quad (25)$$

and making the analogous modification to the combination $\kappa + 4\mu/3$ (using Q_{p0} instead of Q_{s0}). Equation (25) can be derived from the equation (9) of D98 by setting the relaxation spectrum to the constant $1/\ln(\tau_M/\tau_m)$ and carrying out the integration over the interval ($\ln \tau_m$, $\ln \tau_M$). For both the wavenumber-integration and FD solutions, we adjusted the infinite-frequency moduli, μ_u and $\kappa_u + 4\mu_u/3$, such that the (frequency-dependent) *P*- and S-wave phase velocities equal the target wavespeeds, α and β, respectively, at a reference frequency of 10 Hz.

Figure 5 shows the results for the anelastic solution with Q_{p0} and Q_{s0} equal to 50. The FD solution is free of any visible spurious oscillations and reproduces the wavenumber-integration solution with considerable precision. This agreement is even better than in the infinite Q case, since attenuation has eliminated the spurious high-frequency oscillations without introducing any new numerical artifacts (within the usable bandwidth). This example contains body waves (a *P* wave, arriving at ~1.7 sec, *SV* and *SH* arrivals at ~3.0 sec), a surface-diffracted phase (*SP* arriving at ~2.2 sec) and a surface wave (the Rayleigh wave, arriving at ~3.2 sec). Similar agreement is achieved for each of these wave types. The good numerical results for the *SP* and Rayleigh wave, especially, complement the plane-wave tests by confirming that the attenuation methodology has not visibly degraded the performance of the numerical free-surface boundary condition.

To underscore the latter point, we present the elastic and anelastic solutions for a different moment rate function in Figure 6. The source is a twice-differentiated Gaussian (a so-called Ricker wavelet), with the spread *S* set to 0.06 sec. The resulting source has a peaked spectrum that emphasizes the frequency band at which numerical dispersion has become significant, while remaining acceptable for most practical applications (for reference, 0.2-sec period corresponds to about seven grid cells per *S* wavelength). The figure shows the radial velocity component over a time window containing the *SV* and Rayleigh phases. The addition of attenuation via the coarse-grain representation clearly has not degraded

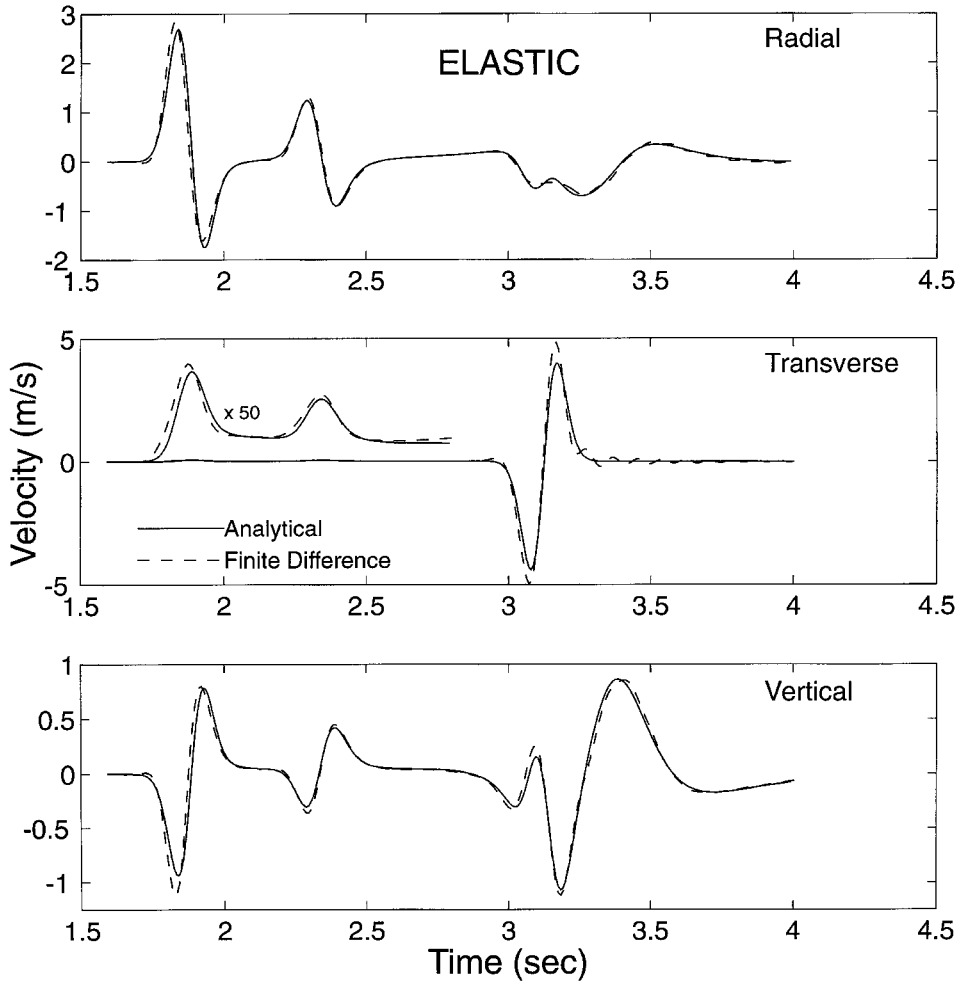

Figure 4. Elastic (infinite Q) solution for the half-space problem with the Gaussian source function. The FD solution (dashed curves) is compared with a reference solution obtained by wavenumber integration (solid curves). The source spectrum was intentionally expanded up to the threshold at which artifacts due to numerical dispersion become visible. This effect is most apparent in the transverse component following the arrival at about 3 sec of the *SH* phase. The early part of the transverse component has been expanded by a factor of 50 to make visible the small near-field phases that precede *SH*.

the performance of the FD method, whether that performance is assessed by qualitative visual agreement with the analytical solution or by quantitative measures such as relative errors of peak amplitudes or phase delays.

Discussion

The foregoing examples confirm the expectation expressed in D98 that the coarse-grain method would work approximately as well for anelastic-wave propagation as for the acoustic-wave case. The plane-wave numerical examples achieve accurate simulation of frequency-independent Q over approximately two decades of frequency using only one memory variable per stress component. The good performance for plane waves appears to carry over to evanescent waves as well, as indicated by the accurate reproduction of all phases, including the Rayleigh wave, in the half-space test. With adjustment of the τ values and w values it should be possible to achieve comparable accuracy for other relaxation models such as the power law $Q(\omega)$.

The tests in this article and in D98 were for a FD method, and it would be useful also to develop and test pseudospectral, finite-element, and spectral-element implementations. We anticipate that the method will perform similarly in any structured-grid scheme, including staggered-grid Fourier pseudospectral implementation. Since the coarse structure of the memory variables generates artifacts at wavelengths shorter than four grid spacings, the suitability of coarse-graining for anelastic pseudospectral calculations hinges upon whether those artifacts entail a loss of usable bandwidth. Our own experience (Xu *et al.,* 1999) has been

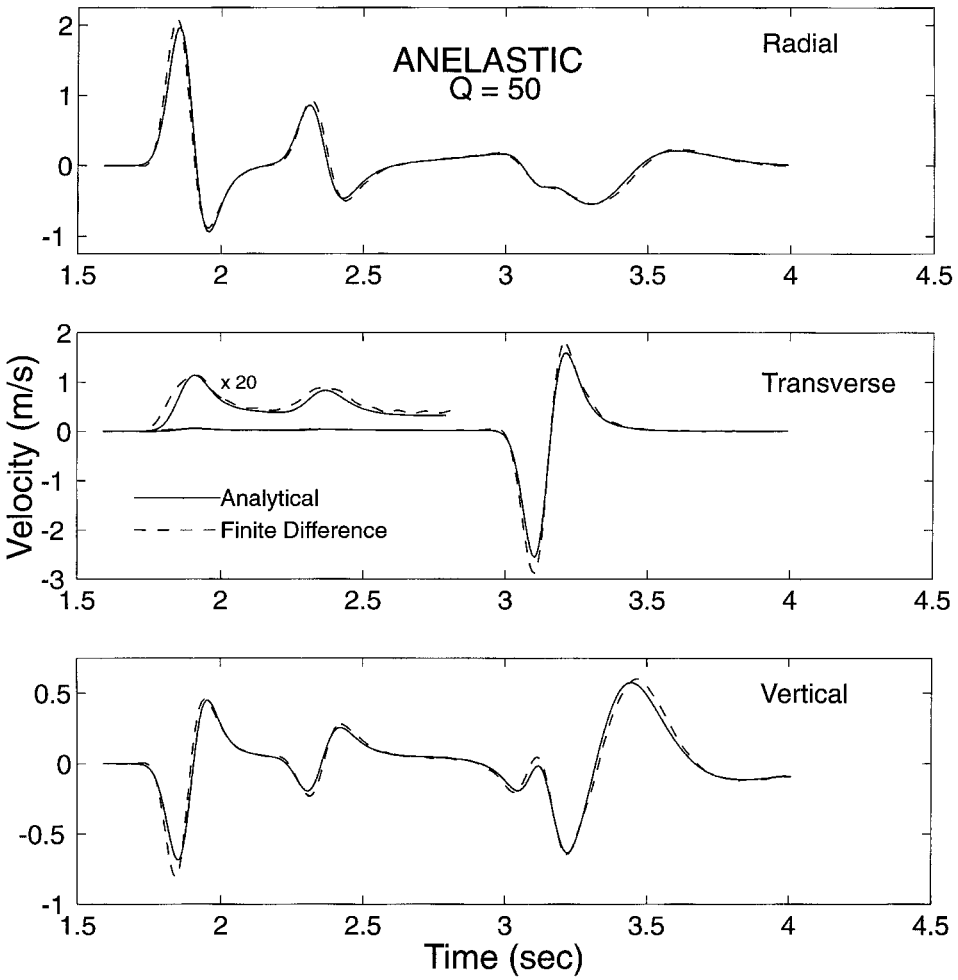

Figure 5. Anelastic solution ($Q_s = Q_p = 50$) for the half-space problem with Gaussian source function. The FD solution (dashed curves) is compared with a reference solution obtained by wavenumber integration (solid curves). The source is identical to that used for the infinite Q solution shown in the previous figure.

that the free-surface boundary conditions limit the short wavelength accuracy of pseudospectral calculations, and wavelengths of four grids may lie outside the usable bandwidth for some applications, making the coarse-grain scheme attractive. In any event, implementing coarse-grain relaxations in pseudospectral codes will be straightforward, following a recipe virtually identical to the FD case presented in this article.

The implementation on a structured grid, as in our FD example, is especially simple, because the relaxation time index at a stress node can be evaluated quickly just from the parities of the three lattice indices (i.e., equation 18). For methods using unstructured meshes, such as most finite-element and spectral-element methods, some alternative approach will have to be devised to associate each stress node with its corresponding relaxation time index. It is also conceivable that mesh irregularity will degrade performance of the coarse-grain approach in finite-element and spectral-element codes, and this possibility will have to be addressed through numerical testing. These two issues, index association and mesh irregularity, are not likely to be fundamental obstacles, and the coarse-graining method is likely to provide the same level of memory savings for the unstructured-grid methods as it does for the FD method.

D98 noted that the relaxation times and weights can be varied to optimize the accuracy with which the target $Q(\omega)$ is fit. Liu and Archuleta (1999) have successfully combined the method of D98 with an optimization scheme for the τ values and w values based on simulated annealing. In case of frequency-independent Q, the resulting optimized τ values still roughly follow the logarithmic distribution used in this article and in D98, but the extra degrees of freedom provided by the w values lead to an improved fit to the target Q. The approach of Liu and Archuleta (1999) may be useful in constructing prescribed frequency-dependent $Q(\omega)$ functions.

Finally, we note that coarse representation of the anelastic memory variables is by no means the only promising

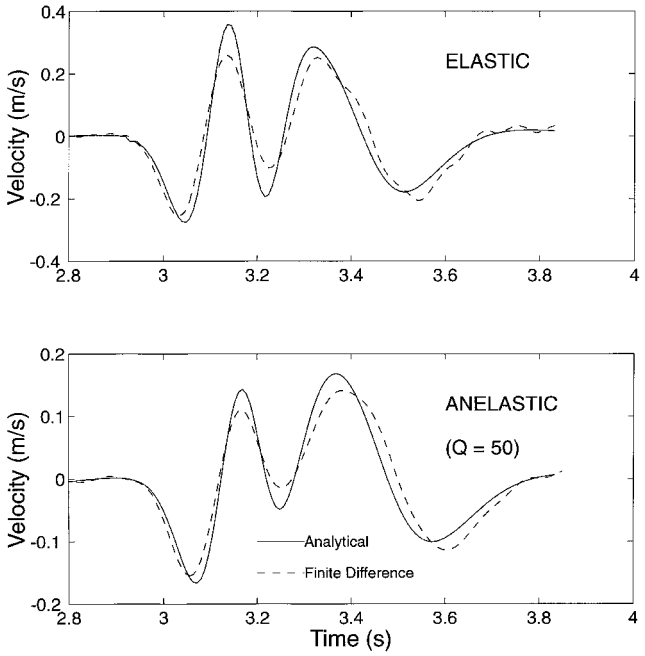

Figure 6. Elastic (infinite Q) and anelastic (Q_s = Q_p = 50) solutions for the half-space problem, radial component, with narrowband (Ricker) source function. The time window shown includes the *SV* and Rayleigh phases.

approach to memory optimization. For example, Graves (1996) achieves very large reduction factors in RAM requirements for FD computation by relying on disk storage for the field variables while maximizing the ratio of computations to disk I/O. Moczo *et al.* (1999) use a lossy compression scheme based on a discrete wavelet transform to optimize RAM and disk storage requirements. Combining the compression scheme with the memory optimization of Graves and the memory variable economization of D98, Moczo *et al.* (2000) in some cases achieve total (disk plus RAM) storage reductions approaching or exceeding an order of magnitude.

Conclusions

We have developed and tested an anelastic generalization of the coarse-grain memory variables scheme proposed by D98 for simulating realistic, broadband attenuation in 3D. The scheme requires only one memory variable per stress component per unit cell. We describe its implementation in logically rectangular, structured-grid FD codes, and we perform tests calculations for the particular case of a fourth-order, staggered, velocity-stress code. For plane *P*- and *S*-wave test cases, the scheme simulates frequency-independent Q to within a 4% tolerance over a frequency band of approximately two decades. Bias from the specified target value of Q was also less than 4%. This accuracy is comparable to that achieved by D98 for acoustic waves, and further improvement, if required, can be achieved easily by optimizing the weights and/or relaxation times. A test calculation for a uniform half-space confirms that the scheme also performs well for elastic waves, such as the Rayleigh wave, that are strongly influenced by the free-surface boundary condition. The coarse-grain scheme may also be applicable to numerical wave-propagation methods on unstructured grids, including finite-element and spectral-element methods, though additional numerical testing will be required to establish accuracy in the presence of grid irregularity.

Acknowledgments

We thank Kim Olsen for allowing us to use his FD source code. We also benefited from discussions of the computational issues with Kim Olsen, Robert Graves, and Peter Moczo. Reviews of the manuscript by Peng-Cheng Liu and Robert Graves led to significant improvements. This work was supported by the Los Alamos National Laboratory (US DOE contract No. W-7405-ENG-36), the National Science Foundation (grant No. CMS-99800663), and the Southern California Earthquake Center (SCEC). SCEC is funded by NSF Cooperative Agreement EAR-8920136 and USGS Cooperative Agreement 14-08-0001-A0899 and 1434-HQ-97AG01718. The SCEC contribution number for this article is 519.

References

Al-Kahtib, H. H., and B. J. Mitchell (1991). Upper mantle anelasticity and tectonic evolution of the Western United States from surface wave attenuation, *J. Geophys. Res.* **96,** no. B11, 18,129–18,146.

Apsel, R. J., and J. E. Luco (1983). On the Green's functions for a layered half-space. Part II, *Bull. Seism. Soc. Am.* **73,** 931–951.

Blanch, J. O., J. O. A. Robertsson, and W. W. Symes (1995). Modeling of a constant Q: methodology and algorithm for an efficient and optimally inexpensive viscoelastic technique, *Geophysics* **60,** 176–184.

Boore, D. M. (1999). Basin waves on a seafloor recording of the 1990 Upland, California, earthquake: implications for ground motions from a larger earthquake, *Bull. Seism. Soc. Am.* **89,** 317–324.

Carcione, J. M., D. Kosloff, and R. Kosloff (1988). Wave propagation in a linear viscoacoustic medium, *Geophy. J. R. Astr. Soc.* **93,** 393–407.

Carcione, J. M., D. Kosloff, A. Behle, and G. Seriani (1992). A spectral scheme for wave propagation simulation in 3-D elastic-anisotropic media, *Geophysics* **57,** 1593–1607.

Chaljub, E., and J.-P. Vilotte (1998). 3D wave propagation in a spherical earth model using the spectral element method, *EOS* **79,** F625–F626.

Day, S. M. (1998). Efficient simulation of constant Q using coarse-grained memory variables, *Bull. Seism. Soc. Am.* **88,** 1051–1062.

Day, S. M., and J. B. Minster (1984). Numerical simulation of attenuated wavefields using a Padé approximant method, *Geophys. J. R. Astr. Soc.* **78,** 105–118.

Emmerich, H., and Korn, M. (1987). Incorporation of attenuation into time-domain computations of seismic wavefields, *Geophysics* **52,** 1252–1264.

Field, E. H. (1996). Spectral amplification in a sediment-filled valley exhibiting clear basin-edge-induced waves, *Bull. Seism. Soc. Am.* **86,** 991–1005.

Frankel, A., and J. Vidale (1992). A three-dimensional simulation of seismic waves in the Santa Clara Valley, California, from a Loma Prieta aftershock, *Bull. Seism. Soc. Am.* **82,** 2045–2074.

Graves, R. W. (1996). Simulating seismic wave propagation in 3D elastic media using staggered-grid finite differences, *Bull. Seism. Soc. Am.* **86,** 1091–1106.

Igel, H., and M. Weber (1995). SH-wave propagation in the whole mantle using high-order finite differences, *Geophys. Res. Lett.* **22,** 731–734.

Jones, E. M., C. R. Bradley, F. N. App, R. J. Bos, and H. J. Patton (1998).

Modeling seismic propagation effects from large scale structural features in western China, LA-UR-97-4186, Los Alamos Manuscript, 97 pp.

Komatitsch, D., and J. Tromp (2000). Numerical modeling of wave propagation in 3D complex media: recent advances using the spectral element method, *Seism. Res. Lett.* **71,** 253.

Krebs, E. S., and G. Quiroga-Goode (1994). A standard finite-difference scheme for the time-domain computation of anelastic wavefields, *Geophysics* **59,** 290–296.

Liu, P. C., and R. J. Archuleta (1999). Modeling of absorbing boundaries and Q for 3-D numerical computations (abstract), in *Proc. of Southern California Earthquake Center Annual Meeting,* Palm Springs, California, 29–30 September.

Lomnitz, C. (1957). Linear dissipation in solids, *J. Appl. Phys.* **28,** 201–205.

Mitchell, B. J., P. Yu, J. Xie, and L. Gong (1997). Lg coda Q variation across Eurasia and its relation to crustal evolution, *J. Geophys. Res.* **102,** no. B10, 22,767–22,779.

Moczo, P., M. Lucka, J. Kristek, and M. Kristekova (1999). 3D displacement finite differences and a combined memory optimization, *Bull. Seism. Soc. Am.* **89,** 69–79.

Moczo, P., J. Kristek, and E. Bystricky (2000). Efficiency and optimization of the 3D finite-difference modeling of seismic ground motion, *J. Comp. Acoustics* (in press).

Nowick, A. S., and B. S. Berry (1972). *Anelastic Relaxation in Crystalline Solids,* Academic Press, New York.

Olsen, K. B. (1994). Simulation of three-dimensional wave propagation in the Salt Lake Basin, *Ph.D. Thesis,* University of Utah, Salt Lake City, Utah, 157 pp.

Olsen, K. B., and R. J. Archuleta (1996). Three-dimensional simulation of earthquakes on the Los Angeles fault system, *Bull. Seism. Soc. Am.* **86,** 575–596.

Olsen, K. B., R. Nigbor, and T. Konno (2000). 3D Viscoelastic wave propagation in the upper Borrego Valley, California, constrained by borehole and surface data, *Bull. Seism. Soc. Am.* **90,** 134–150.

Pitarka, A., K. Irikura, T. Iwata, and H. Sekiguchi (1998). Three-dimensional simulation of the near-fault ground motion for the 1995 Kyogo-ken Nanbu (Kobe), Japan, earthquake, *Bull. Seism. Soc. Am.* **88,** 428–440.

Robertsson, J. O. A., J. O. Blanch, and W. W. Symes (1994). Viscoelastic finite-difference modeling, *Geophysics* **59,** 1444–1456.

Sato, T., R. W. Graves, and P. G. Somerville (1999). Three-dimensional finite-difference simulations of long-period strong motions in the Tokyo metropolitan area during the 1990 Odawara Earthquake (M_J 5.1) and the Great 1923 Kanto Earthquake (M_S 8.2) in Japan, *Bull. Seism. Soc. Am.* **89,** 579–607.

Wald, D. J., and R. W. Graves (1998). The seismic response of the Los Angeles basin, California, *Bull. Seism. Soc. Am.* **88,** 337–356.

Witte, D. C., and P. G. Richards (1990). The pseudospectral method for simulating wave propagation, in *Computational Acoustics: Proceedings of the 2nd IMACS Symposium on Computational Acoustics,* D. Lee, R. Cakmak, and R. Vichnevetsky (Editors), North-Holland, New York, 1–18.

Xu, H., S. M. Day, and J. B. Minster (1999). Two-dimensional linear and nonlinear wave propagation in a halfspace, *Bull. Seism. Soc. Am.* **89,** 903–917.

Xu, T., and G. A. McMechan (1995). Composite memory variables for viscoelastic synthetic seismograms, *Geophys. J. Int.* **121,** 634–639.

Yomogida, K., and J. T. Etgen (1993). 3D wave propagation in the Los Angeles Basin for the Whittier-Narrows earthquake, *Bull. Seism. Soc. Am.* **83,** 1325–1344.

Yoon, K.-H., and G. A. McMechan (1995). Simulation of long-period 3-D elastic responses for whole earth models, *Geophys J. Int.* **120,** 721–730.

Appendix

We write versions of (11) and (12) for mean stress $\bar{\sigma}$, in terms of volumetric strain ε_{kk} and associated memory variable $\bar{\zeta}$, and do the same for deviatoric stresses σ'_{ij} in terms of deviatoric strains ε'_{ij} and associated memory variables ζ'_{ij}:

$$\tau \frac{d\bar{\zeta}}{dt} + \bar{\zeta} = w \frac{\delta\kappa}{\kappa_u} \varepsilon_{kk} \tag{A1a}$$

$$\tau \frac{d\zeta'_{ij}}{dt} + \zeta'_{ij} = w \frac{\delta\mu}{\mu_u} \varepsilon'_{ij} \tag{A1b}$$

$$\bar{\sigma} = \kappa_u[\varepsilon_{kk} - \bar{\zeta}] \tag{A2a}$$

$$\sigma'_{ij} = 2\mu_u[\varepsilon'_{ij} - \zeta'_{ij}]. \tag{A2b}$$

Noting that the (total) stress tensor components, σ_{ij}, are equal to $\sigma'_{ij} + \bar{\sigma}\delta_{ij}$, we define new variables ξ_{ij}:

$$\xi_{ij} = 2\mu_u\zeta'_{ij} + \kappa_u\bar{\zeta}. \tag{A3}$$

Since τ and w take the same values in (A1a) and (A1b), respectively (as a consequence of our assumption that Q_κ and Q_μ have identical frequency dependence), ξ_{ij} satisfies

$$\tau \frac{d\xi_{ij}}{dt} + \xi_{ij} = w \left[2\delta\mu\varepsilon_{ij} + \left(\delta\kappa - \tfrac{2}{3}\delta\mu\right)\varepsilon_{kk}\delta_{ij} \right] \tag{A4}$$

and

$$\sigma_{ij} = 2\mu_u\varepsilon_{ij} + \left(\kappa_u - \tfrac{2}{3}\mu_u\right)\varepsilon_{kk} - \xi_{ij}. \tag{A5}$$

Finally, we assume that τ and w have been chosen to simulate a relaxation spectrum constant on support interval ($\ln \tau_m$, $\ln \tau_M$), as in D98, and write (A4) in terms of the Q of the P and S waves at reference frequency ω_0, denoted Q_{p0} and Q_{s0}. The latter are obtained from (13) by replacing the modulus κ by $\kappa + \frac{4}{3}\mu$ (for Q_{p0}) or by μ (for Q_{s0}). The results are given by equations (15) to (17).

Department of Geological Sciences
San Diego State University
San Diego, California, 92182
(S.M.D.)

Los Alamos National Laboratory
P.O. Box 1663, MS F665
Los Alamos, New Mexico, 87545
(C.R.B.)

Manuscript received 28 June 2000.